Journal of Hazardous Materials 186 (2011) 84–91

Contents lists available at ScienceDirect

Journal of Hazardous Materials

journal homepage: www.elsevier.com/locate/jhazmat

Three-dimensionally ordered and wormhole-like mesoporous iron oxide catalysts highly active for the oxidation of acetone and methanol

Yunsheng Xia, Hongxing Dai*, Haiyan Jiang, Lei Zhang, Jiguang Deng, Yuxi Liu

Laboratory of Catalysis Chemistry and Nanoscience, Department of Chemistry and Chemical Engineering, College of Environmental and Energy Engineering, Beijing University of Technology, Beijing 100124, PR China

ARTICLE INFO

Article history:
Received 12 August 2010
Received in revised form
30 September 2010
Accepted 19 October 2010
Available online 25 October 2010

Keywords:
Three-dimensional mesoporous iron oxide
Hard-templating fabrication
Citric acid-complexing method
Volatile organic compounds
Catalytic oxidation

ABSTRACT

Three-dimensionally (3D) ordered and wormhole-like mesoporous iron oxides (denoted as Fe-KIT6 and Fe-CA) were respectively prepared by adopting the 3D ordered mesoporous silica KIT-6-templating and modified citric acid-complexing strategies, and characterized by a number of analytical techniques. It is shown that the Fe-KIT6-400 and Fe-CA-400 catalysts derived after 400 °C-calcination possessed high surface areas (113–165 m^2/g), high surface adsorbed oxygen concentrations, and good low-temperature reducibility, giving 90% conversion below 189 and 208 °C for acetone and methanol oxidation at 20,000 mL/(g h), respectively. It is believed that the good catalytic performance of Fe-CA-400 and Fe-KIT6-400 was related to factors such as higher surface area and oxygen adspecies concentration, better low-temperature reducibility, and 3D mesoporous architecture.

1. Introduction

Volatile organic compounds (VOCs), such as alcohols, ketones, aldehydes, esters, and aromatics, are emitted into the atmosphere in large quantity due to human activities. Most of the VOCs are pollutants to human health and the atmospheric environment. Various methods, such as adsorption, absorption, pyrolysis, catalytic combustion, and photocatalytic degradation strategies, have been developed for the elimination of harmful VOCs. Among them, the removal of VOCs by means of catalytic combustion is believed to be one of the most effective pathways [1,2]. Nonetheless, the key issue for such an approach is the availability of an effective catalyst. Therefore, developing novel and high-performance catalytic materials is a big challenge in controlling VOCs emissions.

In the past years, supported noble metals, perovskite-type oxides, and single or mixed transition-metal oxides have been utilized to catalyze the combustion of VOCs. Despite the effectiveness of supported noble metals, the high cost and limited availability of precious metals restrict their wide applications. It is cheaper to use base metal oxide catalysts, but good performance is only observed at much higher temperatures, inevitably resulting in high energy consumption and fast deactivation of catalysts. However, some of transition-metal oxides show good catalytic activities, with the oxides of cobalt, manganese, and chromium performing the best [3–5]. As one of transition-metal oxides, iron oxide and its based materials have recently received much attention in catalysis. For example, in the presence of Fe_2O_3 (surface area = 22 m^2/g), ethanol and propane could be totally oxidized at 300 and 560 °C, respectively, under the conditions of ethanol (or propane)/oxygen volumetric ratio = 1:20.8 or 2:20 and SV = 20,000 mL/(g h) [6].

Up to now, mesoporous (pore diameter = 2–50 nm) transition-metal oxides have been extensively studied for the destruction of VOCs due to their unique physicochemical properties. Mesoporous metal oxide synthesis usually requires structure-directing agents, such as soft templates (e.g., surfactants [7]) and hard templates (e.g., porous carbon [8] and silica [4]). For example, mesoporous chromia with a surface area of 78 m^2/g, over which 94% toluene could be removed at room temperature [9], was generated using triblock copolymer F127 as soft template and chromium nitrate as metal source. Song and co-workers employed cetyltrimethylammonium bromide (CTAB) as soft template, iron nitrate as metal precursor, and urea as precipitating agent to fabricate mesoporous iron oxide with a surface area of 175 m^2/g and an average pore diameter of 2 nm. This material showed good activity in catalyzing the disproportionation of CO [10].

Previously, we investigated a number of catalysts (e.g., $La_{1-x}Sr_xMO_3$ (M = Mn, Co) [11–13] and $LaCoO_3$/SBA-15 [14]), and found that these materials showed excellent catalytic performance for the oxidation of typical VOCs (e.g., toluene and ethyl acetate). Recently, we have extended our attention to the fabrication and

* Corresponding author. Tel.: +86 10 6739 6588; fax: +86 10 6739 1983.
E-mail address: hxdai@bjut.edu.cn (H. Dai).

0304-3894/$ – see front matter © 2010 Elsevier B.V. All rights reserved.
doi:10.1016/j.jhazmat.2010.10.073

catalysis chemistry of mesoporous transition-metal oxides [15]. Herein, we report the facile preparation and catalytic performance for acetone and methanol removal of high-surface-area iron oxides with three-dimensional (3D) ordered and wormhole-like mesoporous structures. It is found that using the facile methods could generate mesoporous iron oxides with higher surface areas and better pore structures; the iron oxide catalysts with wormhole-like mesopores outperformed the counterparts with ordered mesopores prepared after the same thermal treatments. Factors, such as surface area, oxygen adspecies concentration, low-temperature reducibility, and mesoporous structure, have been discussed with the catalytic activity of the porous iron oxides.

2. Experimental

2.1. Catalyst preparation

The hard template, 3D mesoporous silica (KIT-6), was synthesized according to the method described elsewhere [16]. In a typical synthesis of 3D ordered mesoporous iron oxide catalyst, 0.75 g of KIT-6 powders was put in a glass tube, in which there were a branched open end connected to vacuum (0.07 MPa) and another open end sealed by a funnel containing 1.00 g of $Fe(NO_3)_3{\cdot}9H_2O$ and 5 mL of ethanol. After evacuation under vacuum for 10 min, the iron nitrate-containing ethanol solution was added dropwise to the KIT-6 powders. After drying under vacuum and at room temperature (RT), a nearly dried mixture was obtained. The dried mixture was calcined in air at a ramp of 1 °C/min from RT to 300, 400 or 500 °C and kept at this temperature for 3 h. The resulting powders were treated with 6 mL of a 10 wt% HF aqueous solution, centrifuged, washed with deionized water and absolute ethanol three times for the complete removal of the KIT-6 template, and finally dried in air at 60 °C overnight. The obtained catalyst was denoted as Fe-KIT6-300, Fe-KIT6-400, and Fe-KIT6-500, respectively.

The wormhole-like iron oxide catalysts were prepared with ferric nitrate as metal source using a modified citric acid-complexing method. Well grounded $Fe(NO_3)_3{\cdot}9H_2O$ and citric acid monohydrate powders were mixed at a molar ratio of 1:1. The mixture was transferred to a ceramic crucible and then calcined in air at a ramp of 1 °C/min from RT to 300, 400 or 500 °C and kept at this temperature for 3 h. The final product was washed with deionized water, filtered, and dried at 60 °C for 12 h. The as-prepared catalyst was denoted as Fe-CA-300, Fe-CA-400, and Fe-CA-500, respectively.

For comparison purposes, we also prepared the bulk iron oxide (denoted as *bulk*-Fe) catalyst by calcining a certain amount of ferric nitrate at 650 °C in air for 3 h.

All of the chemicals (A.R. in purity) were purchased from Beijing Chemicals Company and used without further purification.

2.2. Catalyst characterization

The catalysts were characterized by means of the techniques, such as X-ray diffraction (XRD), thermogravimetric analysis (TGA), differential scanning calorimetry (DSC), Fourier transform infrared (FT-IR), high-resolution transmission electron microscopy (HRTEM), selected-area electron diffraction (SAED), X-ray photoelectron spectroscopy (XPS), and surface area (BET) and pore size distribution (BJH) measurements. The detailed procedures were described in Supplementary material.

The reducibility of the catalysts was measured by means of hydrogen temperature-programmed reduction (H_2-TPR) on an AutoChem II 2920 (Micromeritics) instrument using a 5% H_2–95% Ar mixture in the range of RT–800 °C. 10–15 mg of the catalyst was placed in a U-shaped quartz tube and purged with a helium flow of 30 mL/min at 200 °C for 1 h. After being cooled to RT in the same atmosphere and switched to a 5% H_2–95% Ar mixture flow of 30 mL/min for purging, the pretreated catalyst was heated at a rate of 10 °C/min from RT to 800 °C. The thermal conductivity detector (TCD) responses were calibrated against that of the complete reduction of a standard CuO powdered sample (Aldrich, 99.995%).

2.3. Catalytic evaluation

Acetone and methanol were chosen as the representative reactants for VOCs combustion. The catalytic activity evaluation was carried out in a quartz fixed-bed micro-reactor (i.d. = 4 mm). The reactant gas mixture was composed of 1000 ppm VOC (acetone or methanol), oxygen, and nitrogen (balance), the VOC/O_2 molar ratio was 1:20. About 0.1 g of the catalyst (40–60 mesh) was diluted with 0.5 g of quartz sands (40–60 mesh) to avoid the occurrence of hotspots, and the SV value was 20,000 mL/(g h). Acetone or methanol concentration in the feed mixture was controlled by the flow rate of balance N_2 that passed through a container filled with acetone or methanol at 0 °C, and the container was immersed in an ice/water bath. To change the SV value, we altered the amount of catalyst. The product gas mixture was analyzed by a gas chromatograph (Shimadzu GC-2010) equipped with a TCD using a Chromosorb 101 column for acetone or methanol and a Carboxen 1000 column for permanent gas separation. The balance of carbon in each run was estimated to be around 99.5%. At the onset of reaction, the catalyst was pretreated with reactant mixture at 150 °C for 1.5 h to prevent overestimation of acetone or methanol conversion caused by the adsorption of the VOC molecules in the initial stages of the test.

3. Results and discussion

3.1. Crystal structure

Fig. 1 shows the XRD patterns of the prepared iron oxide catalysts. By comparing the XRD pattern of the standard iron oxide sample (JCPDS PDF# 87-1164), it can be deduced that the three prepared samples were rhombohedral α-Fe_2O_3 in crystal structure. All of the Bragg diffraction peaks in the 2θ range of 10–80° could be well indexed, as indicated in Fig. 1A(c). There were no significant differences in peak intensity for the three iron oxide catalysts, demonstrating that calcination at a temperature of above 300 °C could guarantee the complete decomposition of iron nitrate. It was also confirmed by the results of TGA/DSC investigations (Fig. 1S Supplementary material). The appearance of a weak diffraction signal at 2θ = ca. 1° for each of the catalysts (Fig. 1B) indicates the formation of ordered mesoporous structure. The Fe_2O_3 catalyst obtained after calcination at 400 °C exhibited the highest intensity of the small-angle XRD signal (Fig. 1B(b)), suggesting that this catalyst possessed the best quality of mesoporous architectures among the three KIT-6-derived catalysts. As for the iron oxide catalysts fabricated via the modified citric acid-complexing route, their diffraction peaks could be indexed to the rhombohedral α-Fe_2O_3 phase (Fig. 2A(c)), and a rise in calcination temperature led to the improvement in crystallinity of α-Fe_2O_3. The FT-IR result (Fig. 2S Supplementary material) reveals the formation of the α-Fe_2O_3 phase and the complete removal of citric acid after the complexed iron intermediate was calcined at 400 °C. However, no significant diffraction signals at 2θ = ca. 1° were detected for the three catalysts fabricated by the modified citric acid-complexing method (Fig. 2B). This result indicates that there was no formation of ordered mesopores [7] in these iron oxide catalysts.

3.2. Pore structure

Shown in Fig. 3 are the representative N_2 adsorption-desorption isotherms and pore size distributions of the Fe-KIT6-400 and Fe-

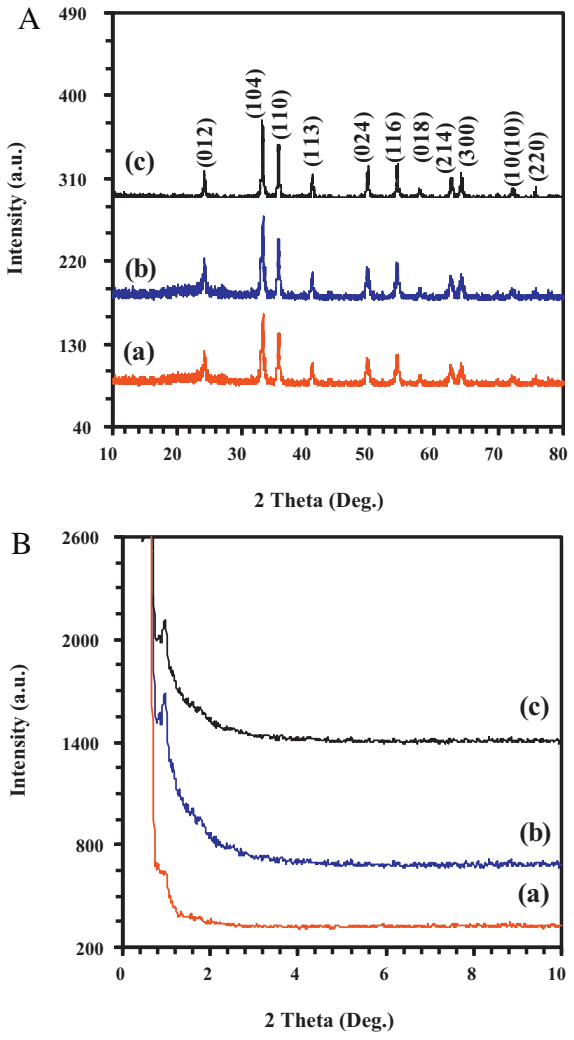

Fig. 1. (A) Wide-angle and (B) small-angle XRD patterns of (a) Fe-KIT6-300, (b) Fe-KIT6-400, and (c) Fe-KIT6-500.

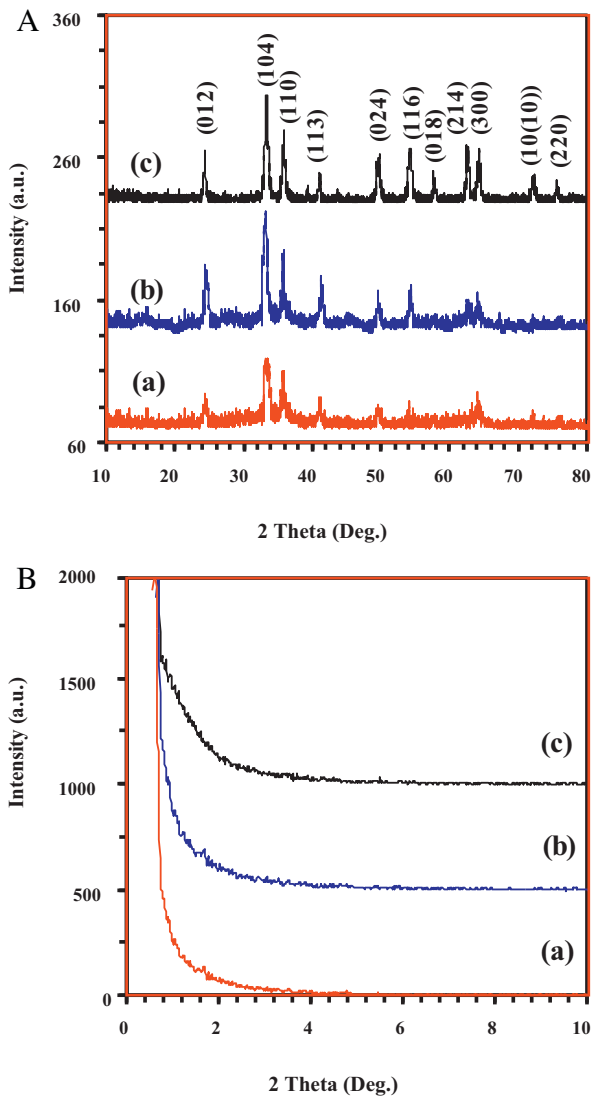

Fig. 2. (A) Wide-angle and (B) small-angle XRD patterns of (a) Fe-CA-300, (b) Fe-CA-400, and (c) Fe-CA-500.

CA-400 catalysts. A H2 type hysteresis loop was observed in the p/p_0 range of 0.45–0.95 for the Fe-KIT6-400 catalyst and in the p/p_0 range of 0.40–0.95 for the Fe-CA-400 catalyst. Similar isotherms also appeared for mesoporous iron oxide, cobalt oxide, and nickel oxide prepared using the nanocasting method with different hard templates [17–20]. Such a deduction was confirmed by the results of pore size distribution measurements (insets of Fig. 3). There were two peaks centered at pore size = 3.7 and 10.9 nm for the Fe-KIT-6-400 catalyst and two peaks centered at pore size = 3.5 and 5.9 nm for the Fe-CA-400 catalyst. It should be noted that, in addition to mesopores, the Fe-CA-400 catalyst might also contain some micropores since the dV/dD value decreased with increasing pore size in the range of 0–2 nm (inset of Fig. 3b). Table 1 lists the textural parame-

Table 1
Pore structure parameters of the prepared catalysts.

Catalyst	BET surface area (m^2/g)	Average pore diameter (nm)	Pore volume (cm^3/g)
Fe-KIT6-300	96	9.3	0.16
Fe-KIT6-400	113	8.5	0.18
Fe-KIT6-500	87	11.7	0.20
Fe-CA-300	131	4.2	0.19
Fe-CA-400	165	3.9	0.17
Fe-CA-500	107	4.8	0.21
bulk-Fe	7	–	–

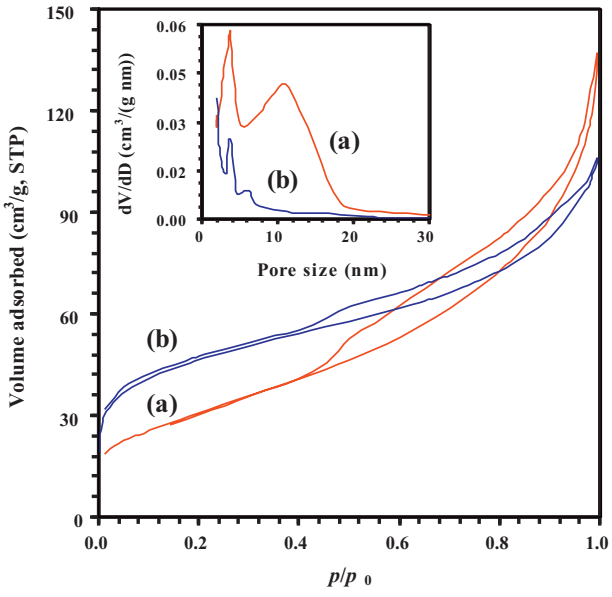

Fig. 3. N_2 adsorption–desorption isotherms and pore size distributions (insets) of (a) Fe-KIT6-400 and (b) Fe-CA-400.

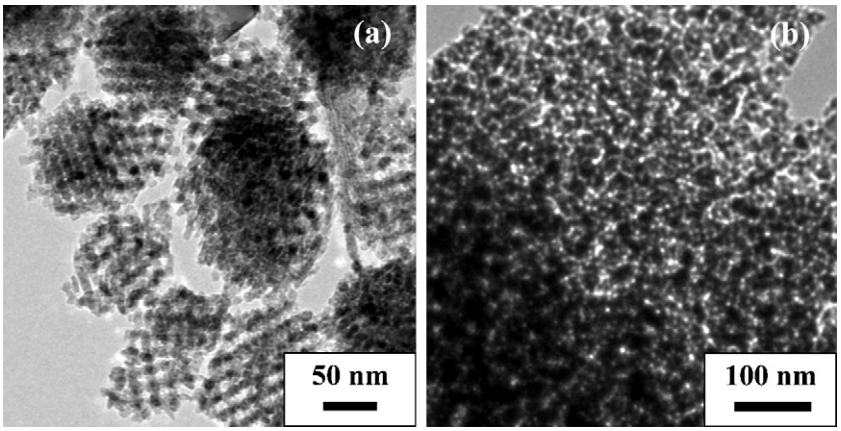

Fig. 4. HRTEM images of (a) Fe-KIT6-400 and (b) Fe-CA-400.

ters of the as-prepared catalysts. It can be observed that the surface areas (87–165 m^2/g) of the iron oxide catalysts prepared either by the KIT-6 templating method or by the modified citric acid-complexing method were much higher than that (7 m^2/g) of the *bulk*-Fe catalyst. For the KIT-6- or CA-derived catalysts, with the rise in calcination temperature, the surface area first increased and then decreased, with the highest surface area (113 m^2/g for Fe-KIT6-400 and 165 m^2/g for Fe-CA-400) and the smallest pore size (8.5 nm for Fe-KIT6-400 and 3.9 nm for Fe-CA-400) being achieved at a calcination temperature of 400 °C. No significant changes in pore volume were observed with the rise in calcination temperature.

Fig. 4 shows the TEM images of the Fe-KIT6-400 and Fe-CA-400 catalysts. It is clearly observed that there were a number of iron oxide entities with ordered mesopores, and the pore size was in the range of 4–10 nm (Fig. 4a). The mesopores and their walls were formed due to the removal of the silica in the mesoporous walls of KIT-6 and the decomposition of ferric nitrate filled in the mesopores of KIT-6, respectively. Fig. 3S shows the HRTEM images of the Fe-KIT6-400 and Fe-CA-400 catalysts. The lattice spacing *d* value of the (1 0 4) plane was estimated to be 0.27 nm, rather close to that (0.269895 nm) of α-Fe_2O_3 (JCPDS PDF# 87-1164). This result means that the mesopore walls were crystalline α-Fe_2O_3. As shown in the SAED pattern of Fe-KIT6-400 (inset of Fig. 3S(a)), there were multiple bright electron diffraction rings, indicating the generation of polycrystalline iron oxide. As for the Fe-CA-400 catalyst, however, there was formation of wormhole-like mesopores (Fig. 4b). By employing the citric acid-assisted thermal decomposition, Li et al. [20] obtained chromia with a wormhole-like mesoporous structure. The pore walls of Fe-CA-400 were also polycrystalline, as revealed from the SAED pattern (inset of Fig. 3S(b)), and the *d* value of the (1 0 4) crystal plane was not far away from that of the standard iron oxide sample (JCPDS PDF# 87-1164). Similar TEM images and SAED patterns were recorded for the other iron oxide catalysts.

3.3. Surface composition and reducibility

Figs. 5 and S4 show the Fe 2p and O 1s XPS spectra of the *bulk*-Fe, Fe-KIT6-400, and Fe-CA-400 catalysts. There were two strong signals centered at BE = 711.0 and 723.0 eV assignable to Fe $2p_{3/2}$ and Fe $2p_{1/2}$, respectively, and a weak satellite signal at BE = 719.0 eV due to Fe^{2+} (Fig. 4S). Similar XPS spectra of α-Fe_2O_3 had also been reported by other authors [21,22]. As shown in Fig. 5A, the asymmetrical Fe $2p_{3/2}$ XPS peak of each catalyst could be decomposed to two components at BE = 710.0–710.4 and 711.3–711.9 eV, ascribable to the Fe^{2+} and Fe^{3+} signals [21,23–25], respectively. From Fig. 5B, one can see an asymmetrical O 1s XPS peak of each catalyst that could be resolved into two components at BE = 529.5–529.9 and 531.1–531.7 eV; the former was due to the surface lattice oxygen (O_{latt}) species whereas the latter was due to the surface adsorbed oxygen (O_{ads}) species [24,25]. The surface iron and oxygen compositions of *bulk*-Fe, Fe-KIT6-400, and Fe-CA-400 are summarized in Table 2. It is observed that the Fe^{3+}/Fe^{2+} molar ratio (3.40) of *bulk*-Fe was much lower than those (3.85–3.95) of Fe-KIT6-400 and Fe-CA-400; the O_{ads}/O_{latt} molar ratio (0.84) of the former catalyst was markedly lower than those (1.06–1.53) of the latter two catalysts, indicating that the porous iron oxide catalysts possessed much more oxygen adspecies than the nonporous counterpart.

Reducibility of transition-metal oxide catalysts is an important factor in influencing their catalytic performance. It is known that the reduction of iron oxide proceeds at elevated temperatures according to the sequence of α-$Fe_2O_3 \rightarrow Fe_3O_4 \rightarrow Fe^0$ [23]. Fig. 6A illustrates the H_2-TPR profiles of the prepared catalysts. For each catalyst, two reduction steps were observed in the range of 190–320 and 320–600 °C, respectively. The former step was due to the reduction of α-Fe_2O_3 to Fe_3O_4 [26,27], whereas the latter step originated from the reduction of Fe_3O_4 to Fe^0 [23,26,27]. After quantifying the reduction bands, for the *bulk*-Fe, Fe-KIT6-300, Fe-KIT6-400, Fe-KIT6-500, Fe-CA-300, Fe-CA-400, and Fe-CA-500 catalysts, the H_2 consumption in the low-temperature region (190–320 °C) was 1.65, 1.68, 1.70, 1.68, 1.69, 1.69, and 1.69 mmol/g, whereas that in the high-temperature region (320–600 °C) was 16.09, 16.13, 16.15, 16.13, 16.15, 16.14, and 16.14 mmol/g, respectively. Supposed that (i) all of the iron ions were Fe^{3+} and reduced to Fe^0, the H_2 consumption would be 18.74 mmol/g; and (ii) all of the iron ions were Fe^{2+} and reduced to Fe^0, the H_2 consumption would be 13.89 mmol/g. As revealed in our H_2-TPR results, the H_2 consumption of the iron oxide catalysts was in the range of 17.73–17.85 mmol/g. Obviously, the iron ions in our iron oxide catalysts existed in mixed oxidation states (Fe^{3+} and Fe^{2+}), which was confirmed by the results of XPS investigations (Fig. 5A).

In order to gain a better understanding on the reducibility of the catalysts, we used the initial (i.e., less than 25% oxygen in iron oxide was consumed for the first reduction band) H_2 consumption rate to evaluate the catalyst reducibility [28], and the results are shown in Fig. 6B. It is observed that the initial H_2 consumption rates of the catalysts followed a sequence of Fe-CA-400 > Fe-CA-300 > Fe-KIT6-400 > Fe-CA-500 > Fe-KIT6-300 > Fe-KIT6-500 > *bulk*-Fe, coinciding with the order in surface area of the materials.

3.4. Catalytic performance

In the blank experiment (only quartz sand was loaded in the micro-reactor), we detected no significant oxidation of acetone and

Table 2
Surface compositions of the Fe-KIT6-400, Fe-CA-400, and *bulk*-Fe catalysts.

Catalyst	Iron			Oxygen		
	Fe^{2+} (mol%)	Fe^{3+} (mol%)	Fe^{3+}/Fe^{2+}	O_{latt} (mol%)	O_{ads} (mol%)	O_{ads}/O_{latt}
Fe-KIT6-400	20.6	79.4	3.85	48.6	51.4	1.06
Fe-CA-400	20.2	79.8	3.95	39.6	60.4	1.53
bulk-Fe	22.7	77.3	3.40	54.4	45.6	0.84

methanol under the conditions of acetone or methanol concentration = 1000 ppm, acetone (or methanol)/O_2 molar ratio = 1/20, SV = 20,000 mL/(g h), and reaction temperature ≤310 °C. This result indicates that the homogeneous reaction of the VOC molecules were negligible under the reaction conditions adopted in the study. Figs. 7 and 8 show the catalytic activities of Fe-CA-400 and Fe-KIT6-400 versus temperature at 20,000 mL/(g h) or different SV values for acetone and methanol combustion. Obviously, acetone or methanol conversion increased with the rise in temperature or with the drop in SV, and Fe-CA-400 and Fe-KIT6-400 performed the best in each series of the catalysts. Table 1S (see the Supplementary material) summarizes the activities of the prepared catalysts. The reaction temperatures $T_{10\%}$, $T_{50\%}$, and $T_{90\%}$ (corresponding to VOC conversion = 10, 50, and 90%) could be used to evaluate the catalytic performance. Apparently, Fe-CA-400 and Fe-KIT6-400 performed much better than *bulk*-Fe. A $T_{90\%}$ value of 208 °C for acetone oxidation and 204 °C for methanol oxidation was achieved over the Fe-KIT6-400 catalyst, whereas over the Fe-CA-400 catalyst the $T_{90\%}$ value was 186 °C for acetone oxidation and 189 °C for methanol oxidation. It is better to use the VOC reac-

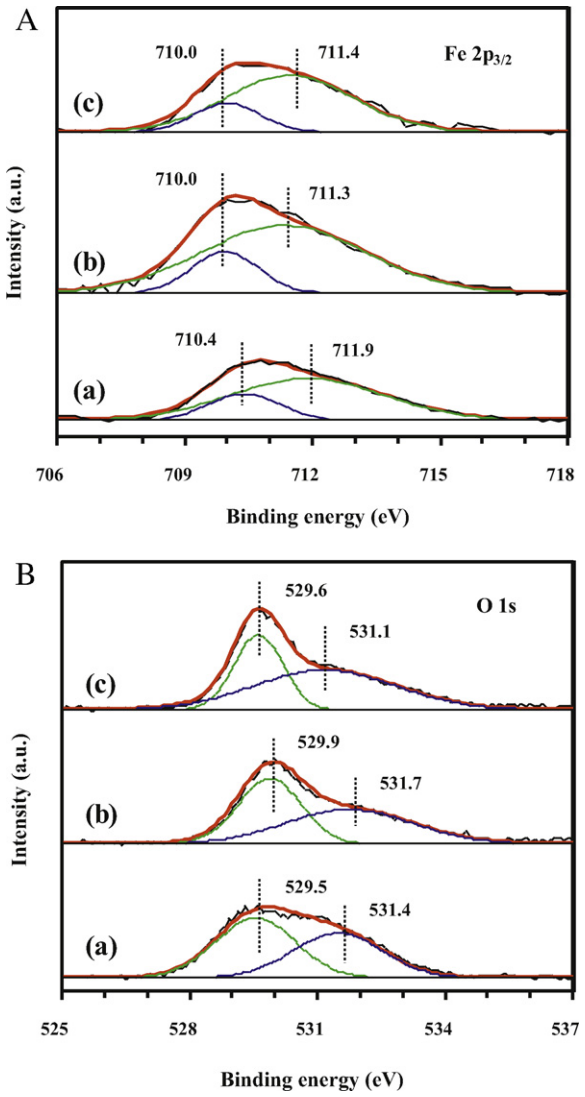

Fig. 5. (A) Fe $2p_{3/2}$ and (B) O 1s XPS spectra of (a) *bulk*-Fe, (b) Fe-KIT6-400, and (c) Fe-CA-400.

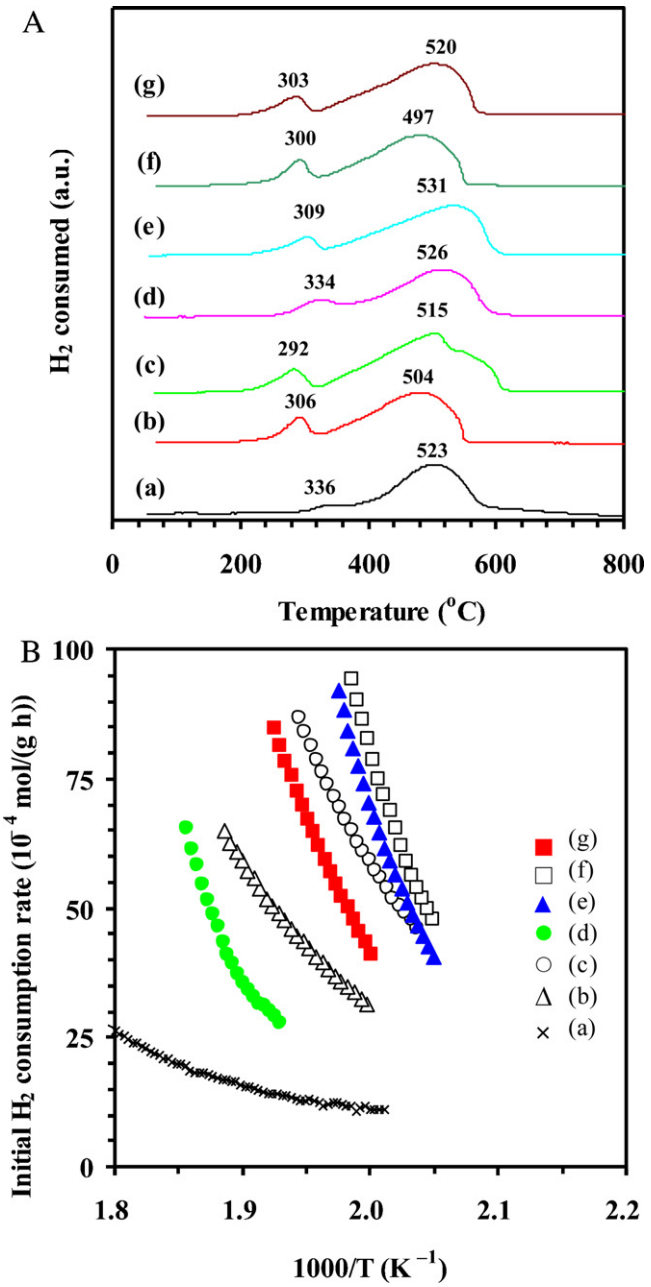

Fig. 6. (A) H_2-TPR profiles and (B) initial H_2 consumption rate as a function of inverse temperature of (a) *bulk*-Fe, (b) Fe-KIT6-300, (c) Fe-KIT6-400, (d) Fe-KIT6-500, (e) Fe-CA-300, (f) Fe-CA-400, and (g) Fe-CA-500.

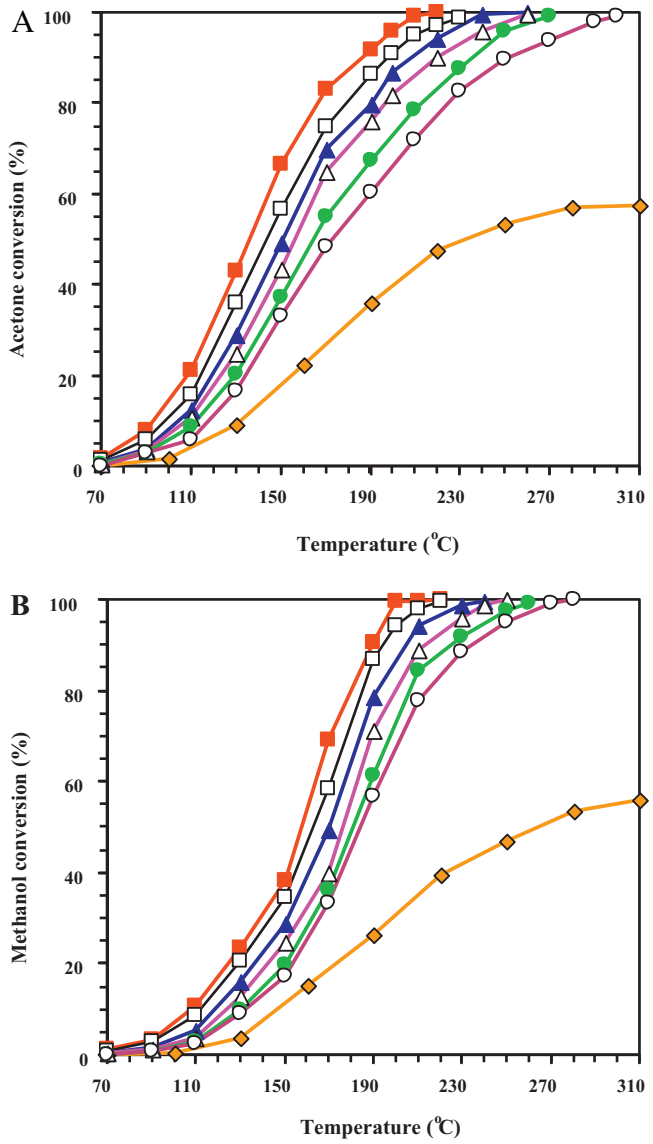

Fig. 7. Catalytic performance as a function of reaction temperature over *bulk*-Fe (♦), Fe-KIT6-300 (●), Fe-KIT6-400 (▲), Fe-KIT6-500 (○), Fe-CA-300 (□), Fe-CA-400 (■), and Fe-CA-500 (△) for the oxidation of acetone (A) and methanol (B) under the conditions of VOC concentration = 1000 ppm, VOC/O_2 molar ratio = 1/20, and SV = 20,000 mL/(g h).

tion rate (calculated from the activity data of Fig. 7) for catalytic performance comparison. Shown in Fig. 5S of the Supplementary material are the reaction rates of acetone and methanol as a function of temperature at 20,000 mL/(g h). Acetone or methanol reaction rate over the *bulk*-Fe catalyst was considerably lower than those over the Fe-KIT6 and Fe-CA serial catalysts above 160 °C. At similar temperatures, the catalytic performance decreased in the order of Fe-CA-400 > Fe-CA-300 > Fe-KIT6-400 > Fe-CA-500 > Fe-KIT6-300 > Fe-KIT6-500 > *bulk*-Fe, in good agreement with the surface area and reducibility sequences of these materials (Table 1 and Fig. 6B). Within 40 h of on-stream reaction, the Fe-CA-400 catalyst displayed a stable performance (Fig. 9). In other words, the mesoporous iron oxide was catalytically durable. It is worth pointing out that acetone and methanol were completely oxidized to CO_2 and H_2O over the prepared iron oxide catalysts, no other incomplete oxidation products were detected in the catalytic system, which was confirmed by the carbon balance of ca. 99.5% in each run.

In the past years, the catalytic removal of acetone or methanol over various catalysts has been investigated. At a space veloc-

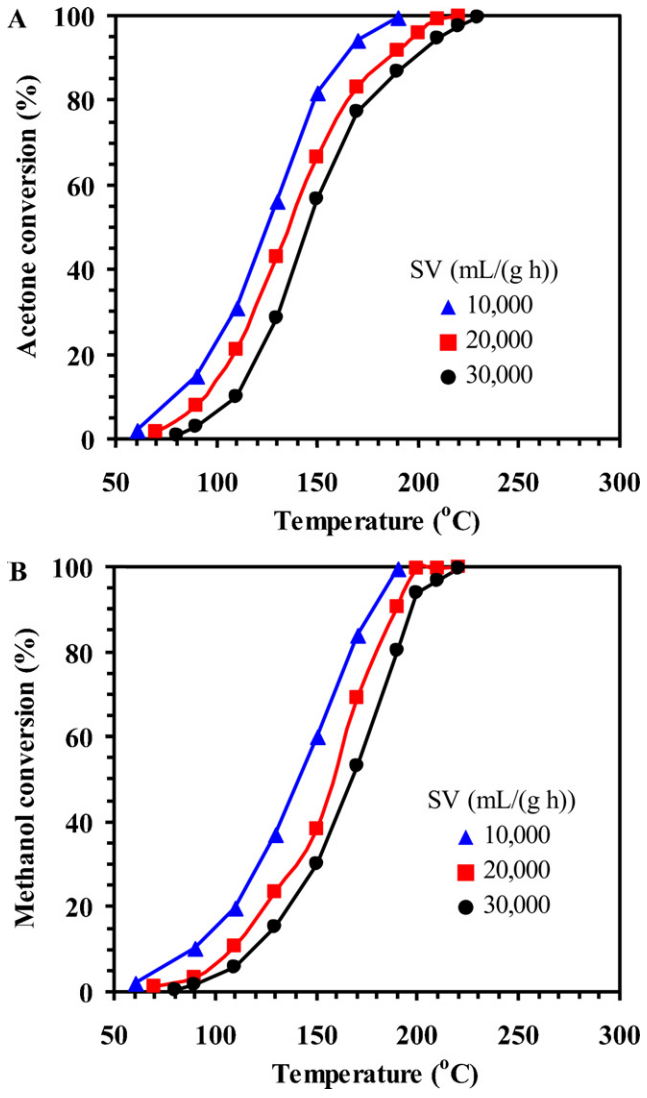

Fig. 8. Effect of SV on the catalytic activity of Fe-CA-400 for the oxidation of (A) acetone and (B) methanol.

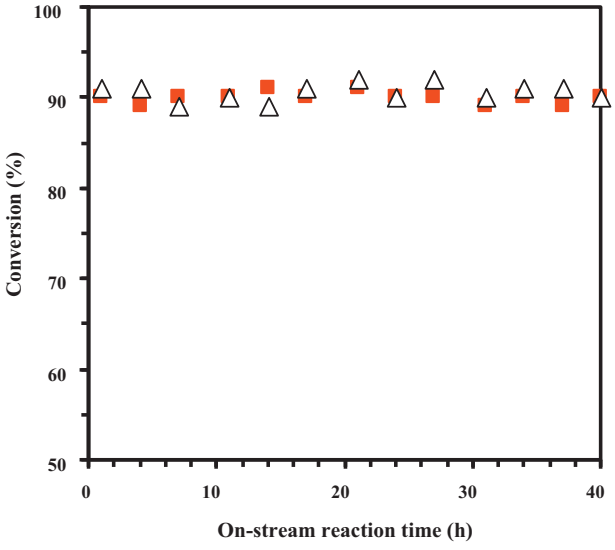

Fig. 9. Catalytic activity versus on-stream reaction time over the Fe-CA-400 catalyst for the oxidation of acetone (■) and methanol (△) at 186 and 189 °C, respectively, at VOC/O_2 molar ratio = 1/20 and SV = 20,000 mL/(g h).

ity of 14,100 h^{-1}, the $T_{50\%}$ and $T_{90\%}$ were 203 and 224 °C over bulk $LaMnO_3$ (surface area = 22 m^2/g), and 222 and 244 °C over bulk $LaCoO_3$ (surface area = 15 m^2/g) [29] for acetone oxidation, respectively. Over the bulk $Cu_{0.13}Ce_{0.87}O_y$ catalyst at space velocity = 15,000 h^{-1} for acetone combustion, the $T_{50\%}$ and $T_{90\%}$ were 200 and 223 °C [30], respectively. Over the 2.1 wt% Au/Fe_2O_3 (surface area = 237 m^2/g) catalyst at space velocity = ca. 170 mL/(g h) for methanol combustion, the $T_{50\%}$ and $T_{90\%}$ were ca. 150 and 190 °C [31], respectively. Usually, the activity of a catalyst is higher at a lower space velocity when other reaction conditions are the same. Obviously, the above-mentioned catalysts were much inferior to Fe-CA-400 and Fe-KIT6-400 in catalytic performance under similar reaction conditions.

It is generally accepted that surface area, surface adsorbed oxygen concentration, reducibility, and pore structure are the key factors influencing the catalytic performance of a transition-metal oxide. By comparing the activity data and characterization results in the present study, it can be realized that there was a clear relationship of the BET surface area (Table 1), adsorbed oxygen concentration (Fig. 5 and Table 2) or low-temperature reducibility (Fig. 6) with the catalytic activity (Figs. 7–9 and S5 and Table 1S). It is well known that the activity of a catalyst would be better if its surface area were higher for the total oxidation of organics [5]. Usually, the oxidation of organic compounds proceeds via the interaction of unadsorbed or adsorbed organic molecules with adsorbed oxygen species [12]. Hence, a higher oxygen adspecies concentration on the catalyst surface is beneficial for the enhancement in catalytic activity [32]. The oxidation of VOCs follows a redox reaction mechanism [33,34], an effective catalyst requires a good reducibility so that high catalytic performance can be achieved. The presence of 3D ordered or wormhole-like mesoporous structure facilitates the adsorption and diffusion of reactant molecules, thus favoring the improvement in catalytic activity [7]. Based on the catalytic data and characterization results as well as the above discussion, we conclude that the good performance of the Fe-KIT6-400 and Fe-CA-400 catalysts was associated with the higher surface area and adsorbed oxygen concentration, better low-temperature reducibility, and 3D mesoporous structure.

4. Conclusions

3D ordered and wormhole-like mesoporous iron oxide catalysts (Fe-KIT6 and Fe-CA) with a rhombohedral crystal structure could be fabricated using the KIT-6-templating and modified citric acid-complexing methods, respectively. All of the catalysts possessed polycrystalline porous walls and high surface areas (87–165 m^2/g). The appropriate calcination temperature was 400 °C for the generation of mesoporous iron oxide that displayed the highest surface area. There was co-presence of Fe^{2+} and Fe^{3+} in the as-fabricated iron oxide catalysts, with the highest surface oxygen adspecies concentration being achieved on the Fe-KIT6-400 and Fe-CA-400 catalysts derived after calcination at 400 °C. Among the iron oxide catalysts, the Fe-CA-400 and Fe-KIT6-400 ones performed the best, giving a $T_{90\%}$ of 186 and 208 °C for acetone oxidation and 189 and 204 °C for methanol oxidation, respectively, under the conditions of VOC concentration = 1000 ppm, VOC/O_2 molar ratio = 1/20, and SV = 20,000 mL/(g h). It is concluded that factors, such as higher surface area and oxygen adspecies concentration, better low-temperature reducibility, and 3D mesoporous structure, accounted for the good catalytic performance of Fe-CA-400 and Fe-KIT6-400.

Acknowledgements

The work described above was supported by the National Natural Science Foundation of China (Nos. 20973017 and 21077007), "863" Key Program of MOST of China (No. 2009AA063201), Creative Research Foundation of Beijing University Technology (No. 00500054R4003), Creative Research Team Foundation of Beijing Municipal Education Commission (Nos. PHR200907105 and PHR201007105), and Natural Science Foundation of Beijing Municipal Education Commission (Key Class B, No. KZ200610005004).

Appendix A. Supplementary material

Supplementary data associated with this article can be found, in the online version, at doi:10.1016/j.jhazmat.2010.10.073.

References

[1] S. Scirè, S. Minicò, C. Crisafulli, C. Satriano, A. Pistone, Catalytic combustion of volatile organic compounds on gold/cerium oxide catalysts, Appl. Catal. B 40 (2003) 43–49.
[2] M.A. Alvarez-Merino, M.F. Ribeiro, J.M. Silva, F. Carrasco-Marín, F.J. Maldonado-Hódar, Activated carbon and tungsten oxide supported on activated carbon catalysts for toluene catalytic combustion, Environ. Sci. Technol. 38 (2004) 4664–4670.
[3] D.C. Kim, S.K. Ihm, Photoreductive dehalogenation of halogenated benzene derivatives using ZnS or CdS nanocrystallites as photocatalysts, Environ. Sci. Technol. 35 (2001) 222–226.
[4] C.M. Pradier, F. Rodrigues, P. Marcus, M.V. Landau, M.L. Kaliya, A. Gutman, M. Herskowitz, Supported chromia catalysts for oxidation of organic compounds: the state of chromia phase and catalytic performance, Appl. Catal. B 27 (2000) 73–85.
[5] H. Rotter, M.V. Landau, M. Carrera, D. Goldfarb, M. Herskowitz, High surface area chromia aerogel efficient catalyst and catalyst support for ethylacetate combustion, Appl. Catal. B 47 (2004) 111–126.
[6] M.R. Morales, B.P. Barbero, L.E. Cadús, Combustion of volatile organic compounds on manganese iron or nickel mixed oxide catalysts, Appl. Catal. B 74 (2007) 1–10.
[7] D.N. Srivastava, N. Perkas, A. Gedanken, I. Felner, Sonochemical synthesis of mesoporous iron oxide and accounts of its magnetic and catalytic properties, J. Phys. Chem. B 106 (2002) 1878–1883.
[8] M. Kang, D. Kim, S.H. Yi, J.U. Han, J.E. Yie, J.M. Kim, Preparation of stable mesoporous inorganic oxides via nano-replication technique, Catal. Today 93–95 (2004) 695–699.
[9] A.K. Sinha, K. Suzuki, Novel mesoporous chromium oxide for VOCs elimination, Appl. Catal. B 70 (2007) 417–422.
[10] Q. Liu, W.M. Zhang, Z.M. Cui, B. Zhang, L.J. Wan, W.G. Song, Aqueous route for mesoporous metal oxides using inorganic metal source and their applications, Micropor. Mesopor. Mater. 100 (2007) 233–240.
[11] J.R. Niu, J.G. Deng, W. Liu, L. Zhang, G.Z. Wang, H.X. Dai, H. He, X.H. Zi, Nanosized perovskite-type oxides $La_{1-x}Sr_xMO_{3-\delta}$ (M = Co, Mn; x = 0, 0.4) for the catalytic removal of ethylacetate, Catal. Today 126 (2007) 420–429.
[12] J.G. Deng, L. Zhang, H.X. Dai, H. He, C.T. Au, Single-crystalline $La_{0.6}Sr_{0.4}CoO_{3-\delta}$ nanowires/nanorods derived hydrothermally without the use of a template: catalysts highly active for toluene complete oxidation, Catal. Lett. 123 (2008) 294–300.
[13] J.G. Deng, Y. Zhang, H.X. Dai, L. Zhang, H. He, C.T. Au, Effect of hydrothermal treatment temperature on the catalytic performance of single-crystalline $La_{0.5}Sr_{0.5}MnO_{3-\delta}$ microcubes for the combustion of toluene, Catal. Today 139 (2008) 82–87.
[14] J.G. Deng, L. Zhang, H.X. Dai, C.T. Au, In situ hydrothermally synthesized mesoporous $LaCoO_3$/SBA-15 catalysts: high activity for the complete oxidation of toluene and ethyl acetate, Appl. Catal. A 352 (2009) 43–49.
[15] Y.S. Xia, H.X. Dai, H.Y. Jiang, J.G. Deng, H. He, C.T. Au, Mesoporous chromia with ordered three-dimensional structure for the complete oxidation of toluene and ethyl acetate, Environ. Sci. Technol. 43 (2009) 8355–8360.
[16] F. Kleitz, S.H. Choi, R. Ryoo, Cubic Ia3d large mesoporous silica: synthesis and replication to platinum nanowires, carbon nanorods and carbon nanotubes, Chem. Commun. (2003) 2136–2137.
[17] F. Jiao, A. Harrison, J.C. Jumas, A.V. Chadwick, W. Kockelmann, P.G. Bruce, J. Am. Chem. Soc. 128 (2006) 5468–5474.
[18] Y. Wang, C.M. Yang, W. Schmidt, B. Spliethoff, E. Bill, F. Schüth, Adv. Mater. 17 (2005) 53–56.
[19] F. Jiao, A.H. Hill, A. Harrison, A. Berko, A.V. Chadwick, P.G. Bruce, Ordered mesoporous Fe_2O_3 with crystalline walls, J. Am. Chem. Soc. 130 (2008) 5262–5266.
[20] L. Li, Z.F. Yan, C.Q. Lu, Z.H. Zhu, Synthesis and structure characterization of chromium oxide prepared by solid thermal decomposition reaction, J. Phys. Chem. B 110 (2006) 178–183.
[21] C.R. Brundle, T.J. Chuang, K. Wandelt, Core and valence level photoemission studies of iron oxide surfaces and the oxidation of iron, Surf. Sci. 68 (1977) 459–468.
[22] M. Muhler, R. Schlögl, S. Eder, G. Ertl, Design of a continuous flow microreactor attached to a surface analysis system: first results with an iron oxide based catalyst, Surf. Sci. 189–190 (1987) 69–79.

[23] C.S. Castro, L.C.A. Olievira, M.C. Guerreiro, Effect of hydrogen treatment on the catalytic activity of iron oxide based materials dispersed over activated carbon: investigations toward hydrogen peroxide decomposition, Catal. Lett. 133 (2009) 41–48.
[24] H.M. Ismail, D.A. Cadenhead, M.I. Zaki, Surface reactivity of iron oxide pigmentary powders toward atmospheric components: XPS, FESEM, and gravimetry of CO and CO_2 adsorption, J. Colloid Interface Sci. 194 (1997) 482–488.
[25] T. Yamashita, P. Hayes, Analysis of XPS spectra of Fe^{2+} and Fe^{3+} ions in oxide materials, Appl. Surf. Sci. 254 (2008) 2441–2449.
[26] E. Rombi, I. Ferino, R. Monaci, C. Picciau, V. Solinas, R. Buzzoni, Toluene ammoxidation on α-Fe_2O_3-based catalysts, Appl. Catal. A 266 (2004) 73–79.
[27] Q. Yang, H. Choi, S.R. Al-Abed, D.D. Dionysiou, Iron–cobalt mixed oxide nanocatalysts: heterogeneous peroxymonosulfate activation, cobalt leaching, and ferromagnetic properties for environmental applications, Appl. Catal. B 88 (2009) 462–469.
[28] H.X. Dai, A.T. Bell, E. Iglesia, Effects of molybdena on the catalytic properties of vanadia domains supported on alumina for oxidative dehydrogenation of propane, J. Catal. 221 (2004) 491–499.
[29] R. Spinicci, M. Faticanti, P. Marini, S. De Rossi, P. Porta, Catalytic activity of $LaMnO_3$ and $LaCoO_3$ perovskites towards VOCs combustion, J. Mol. Catal. A 197 (2003) 147–155.
[30] C.Q. Hu, Q.S. Zhu, Z. Jiang, L. Chen, R.F. Wu, Catalytic combustion of dilute acetone over Cu-doped ceria catalysts, Chem. Eng. J. 152 (2009) 583–590.
[31] S. Minicò, S. Scirè, C. Crisafulli, R. Maggiore, S. Galvagno, Catalytic combustion of volatile organic compounds on gold/iron oxide catalysts, Appl. Catal. B 28 (2000) 245–251.
[32] R.J.H. Voorhoeve, J.P. Remeika, D.W. Johnson, Rare-earth manganites: catalysts with low ammonia yield in the reduction of nitrogen oxides, Science 180 (1973) 62–64.
[33] E. Finocchio, R.J. Willey, G. Busca, V. Lorenzelli, FTIR studies on the selective oxidation and combustion of light hydrocarbons at metal oxide surfaces Part 3. Comparison of the oxidation of C_3 organic compounds over Co_3O_4, $MgCr_2O_4$ and CuO, J. Chem. Soc. Faraday Trans. 93 (1997) 175–180.
[34] M. Baldi, F. Milella, G. Ramis, V. Sanchez Escribano, G. Busca, An FT-IR and flow reactor study of the selective catalytic oxy-dehydrogenation of C_3 alcohols on Mn_3O_4, Appl. Catal. A 166 (1998) 75–88.